Gibbs Films of Semi-Fluorinated Alkanes at the Surface of Alkane Solutions

Piotr Marczuk, Peter Lang,*,† Gerhard H. Findenegg, Surinder K. Mehta, and Martin Möller‡

Stranski Laboratorium für Physikalische und Theoretische Chemie, Technische Universität Berlin, Strasse des 17. Juni 112, 10623 Berlin, Germany

Received January 31, 2002. In Final Form: June 4, 2002

Adsorbed monolayer phases of semi-fluorinated alkanes $F(CF_2)_{12}(CH_2)_mH$ with $m = 12$, 14, 16, and 18 (denoted $F_{12}H_m$) at the free surface of their solutions in H_{12} and H_{16} solvents (dodecane, bicyclohexyl, and hexadecane) were studied by surface tension measurements and surface-sensitive X-ray techniques. Solutions in the two H_{12} solvents exhibit sharp first-order phase transitions from a gaslike state at high temperature to a condensed state at lower temperatures. In the condensed film, the fluorocarbon blocks of the $F_{12}H_m$ molecules are close-packed in two-dimensional hexagonal arrays (cross-sectional area, ca. 28 Å^2), but the in-plane order is rather short ranged, having a positional correlation length of only ca. 20 Å. The electron density profiles $\rho_e(z)$ reveal that the mass centers of the fluorocarbon blocks are not aligned in a plane but distributed over a region of ca. 20−30 Å. The short-range order of these films is attributed to the packing frustration of the different diameters of the fluorocarbon and hydrocarbon blocks of the $F_{12}H_m$ molecules. Gibbs films of $F_{12}H_{16}$ on hexadecane exhibit not a sharp transition but a gradual increase of the surface concentration below 25 °C. This anomalous behavior is attributed tentatively to a solvation of the alkane block of the $F_{12}H_{16}$ molecules by the hydrocarbon solvent, which will prevent a close packing of the fluorocarbon blocks.

Introduction

Semi-fluorinated alkanes (SFA) of the general formula $F(CF_2)_n(CH_2)_mH$ (denoted F_nH_m) are diblock molecules consisting of an oleophobic perfluoroalkane block and an oleophilic alkane block. The mutual antipathy of the hydrocarbon and fluorocarbon chains causes a tendency to demixing of the two blocks and can lead to a self-organization of the SFA in the pure state and in solutions of hydrocarbons. Miscibility studies of hydrocarbon and fluorocarbon solvents have shown[1] that the free energy of transfer of a $-CH_{2-}$ group into fluorocarbon and a $-CF_{2-}$ group into hydrocarbon are approximately 1.1 and 1.4 kJ mol^{-1}, respectively. These values imply that the antipathy between hydrocarbon and fluorocarbon chains is about 1/3 of the free energy of transfer of $-CH_{2-}$ groups from alkane to water, that is, the driving force of the hydrophobic effect. Accordingly, SFAs are expected to be relatively weak amphiphiles in hydrocarbon solvents when compared with conventional surfactants of similar chain length in aqueous media. Weak aggregation of F_nH_m molecules in hydrocarbon solvents, with aggregation numbers in the range 2−10, was observed at concentrations above a critical aggregation concentration (cac) which is generally much higher than the critical micelle concentration of typical surfactants in aqueous solutions. Values of the cac were determined from the temperature dependence of the solubility of the solid SFAs in the hydrocarbon solvents, which exhibits a sharp increase in a narrow temperature range, reminiscent of the Krafft point temperature of surfactants in water.[1]

The structure and thermal behavior of pure SFA in the bulk solid state have been studied in some detail.[2−11] For a series of F_nH_m compounds with $n = 12$ and $m = 6$, 8, 10, and 12, one or more solid/solid phase transitions were found. This structural variety originates not only from the energetic incompatibility of the two blocks but also from their different cross-sectional areas. While the fluorinated block has a cross-sectional area of ca. 28 Å^2 in the solid high-temperature phase,[11] *n*-alkanes in a two-dimensionally ordered surface layer occupy only about 20 Å^2.[12] F_nH_m compounds in their high-temperature bulk solid phase are commonly arranged in monolayer lamellar stacks in which the fluorinated chains are oriented vertical to the planes in a two-dimensional (2D) hexagonal close packing, while the hydrocarbon tails are in a weakly ordered, liquidlike state with a large number of gauche defects along the chain. In this state, the contact area between the fluorinated and hydrogenated blocks of the F_nH_m molecules is minimized and the packing frustration resulting from the spatial incompatibility of the two blocks is relaxed.[11]

Due to their amphiphilic character, solutions of SFA in hydrocarbon solvents exhibit a more or less pronounced

* Corresponding author. E-mail: p.lang@fz-juelich.de.

† Permanent address: Forschungszentrum Jülich, IFF, 52425 Jülich, Germany.

‡ Organische Chemie III Universität Ulm, 89069 Ulm, Germany.

(1) Binks, B. P.; Fletcher, P. D. I.; Kotsev, S. N.; Thompson, R. L. *Langmuir* **1997**, *13*, 6669.

(2) Mahler, W.; Guillon, D.; Skoulios, A. *Mol. Cryst. Liq. Cryst. Lett.* **1985**, *2*, 111.

(3) Rabolt, J. F.; Russell, T. P.; Twieg, R. J. *Macromolecules* **1984**, *17*, 2786.

(4) Russell, T. P.; Rabolt, J. F.; Twieg, R. J.; Siemens, R. L.; Farmer, B. L. *Macromolecules* **1986**, *19*, 1135.

(5) Viney, C.; Russell, T. P.; Depero, L. E.; Twieg, R. J. *Mol. Cryst. Liq. Cryst.* **1989**, *168*, 63.

(6) Viney, C.; Twieg, R. J.; Russell, T. P.; Depero, L. E. *Liq. Cryst.* **1989**, *5*, 1783.

(7) Viney, C.; Twieg, R. J.; Russell, T. P. *Mol. Cryst. Liq. Cryst.* **1990**, *182B*, 291.

(8) Dorset, D. L. *Macromolecules* **1990**, *23*, 894.

(9) Höpken, J. Ph.D. Thesis, Universiteit Twente, Enschede, The Netherlands, 1991.

(10) Lermann, E. Ph.D. Thesis, Universität Ulm, Ulm, Germany, 1997.

(11) Marczuk, P.; Lang, P. *Macromolecules* **1998**, *31*, 9013.

(12) Ocko, B. M.; Wu, X. Z.; Sirota, E. B.; Sinha, S. K.; Gang, O.; Deutsch, M. *Phys. Rev. E* **1997**, *55*, 3164.

10.1021/la025596d CCC: $22.00
Published on Web 08/09/2002

surface activity. Binks et al.[1,13,14] concluded from an analysis of surface tension data that the tendency of F_nH_m molecules to be adsorbed at the hydrocarbon/air interface increases with the antipathy between the fluorinated chain and the hydrocarbon solvent, that is, with increasing chain length of the fluorinated block and increasing carbon number of the hydrocarbon solvent. Hayami and Findenegg[15] studied the temperature dependence of the surface tension of $F_{12}H_{16}$ solutions in hexadecane in the temperature range 15−40 °C, in which no aggregation in the bulk solution occurs. (From the Krafft temperatures of F_8H_{16} and $F_{10}H_{16}$ in hexadecane, 30 and 48 °C, respectively,[1] one expects that the Krafft temperature of $F_{12}H_{16}$ in hexadecane is 60 °C or greater.) Sharp breaks in the temperature derivative of the surface tension were observed, which were attributed to first-order phase transitions in the adsorbed film of $F_{12}H_{16}$. This study indicated striking similarities in the phase behavior between Gibbs films of F_nH_m at the hydrocarbon/air interface and Gibbs films of fatty alcohols and related amphiphiles at the water/air[16] and water/oil[17] interfaces. In the system $F_{12}H_{16}$ + hexadecane, a complication arises from the fact that hexadecane exhibits the phenomenon of surface freezing a few Kelvin above the bulk freezing temperature.[12] It was found that the phase transition of the Gibbs film of $F_{12}H_{16}$ competes with the surface freezing of the pure hexadecane solvent.[15] Also, a pronounced correlation of molecular orientations exists in the liquid state of higher *n*-alkanes such as hexadecane[18] at temperatures near their freezing points. Hence, it was of interest to study the influence of such correlations of molecular orientations of the hydrocarbon solvent on the structure and thermodynamic stability of the Gibbs films of F_nH_m amphiphiles. Such effects can be revealed by comparing the properties of Gibbs films on *n*-alkanes of different chain length as well as branched or cyclic hydrocarbon solvents. It was also of interest to see how the chain length of the hydrocarbon tail of the F_nH_m molecules affects the properties of the Gibbs films in different hydrocarbon solvents.

In this work, we study Gibbs films of a series of $F_{12}H_m$ compounds (m = 12, 14, 16, and 18) at the surface of solutions in three hydrocarbons, *n*-dodecane and bicyclohexyl (H_{12} solvents) and *n*-hexadecane (H_{16} solvent). The experimental temperature range (10−30 °C) is below the estimated Krafft temperature of all these systems, where no aggregation of the SFA in the bulk solution occurs. In addition to surface tension measurements, two complementary surface-sensitive scattering techniques, X-ray reflectometry (XR) and grazing incidence X-ray diffraction (GIXD), are employed.[19−21] In XR, one measures the specular reflectivity of X-rays as a function of the scattering vector q_z normal to the surface. The reflectivity $R(q_z)$ is related to the electron density profile in the direction normal to the surface $\rho_e(z)$. The most commonly used method for the determination of electron density profiles from reflectivity curves is the so-called multibox (or slab) model[19] in which the profiles are analyzed in terms of box height, box density, and the roughness parameter of the interface between adjacent boxes. In the present case, attempts to fit experimental data with curves calculated from a two-box model often yielded roughness parameters which were as large as 30−50% of the height of the neighboring boxes. We therefore applied mainly the model-independent groove tracking method within Parratt's formalism[22,23] which was combined with the simulated annealing technique[24] to avoid local minima.

In GIXD experiments, the angle of incidence of the X-ray beam is below the critical angle of total external reflection. In this case, the transmitted beam degenerates to an evanescent wave which propagates along the surface and is sensitive only to structures within a thin layer close to the sample surface. The scattered intensity is mapped as a function of the scattering vector q_{xy} parallel to the surface and q_z perpendicular to the surface. We have adopted the routines developed for the analysis of GIXD experiments on Langmuir monolayers,[20] where the surface molecules are regarded as cylindrical bodies with their centers of mass arranged in arrays with 2D hexagonal or centered rectangular unit cells. Such ordered surface structures cause Bragg reflexes (rods). The scattered intensity as a function of q_{xy} is related to positional correlations in the surface plane, and the intensity as a function of q_z allows the determination of the tilt directions and tilt angles of the cylinders.

The paper is organized as follows. First, we present surface tension measurements on Gibbs films of $F_{12}H_{18}$ in dodecane and an analysis of the data in terms of the adsorption isotherms and surface phase transition. In the main part of the paper, we report XR and GIXD measurements for Gibbs films of a series of $F_{12}H_m$ materials at the surface of their solutions in dodecane and bicyclohexyl (BCH) and of $F_{12}H_{16}$ on hexadecane. Preliminary results for SFA films on dodecane have been presented elsewhere.[25] The data are analyzed in terms of the thickness and packing density of the Gibbs films at temperatures above and below the surface phase transition. In the Discussion, we elaborate on the peculiarities of these systems and possible reasons for the anomalous behavior of the $F_{12}H_{16}$/hexadecane system, and we compare the behavior of the present Gibbs films adsorbed from dilute solutions with recent results of the surface structure of pure SFA materials at temperatures just above the melting point.[26]

Experimental Section

Materials. The perfluoroalkylalkanes $F_{12}H_{12}$, $F_{12}H_{14}$, $F_{12}H_{16}$, and $F_{12}H_{18}$ were synthesized and purified following the method of Mahler and of Höpken et al.[2,9,27] The solvents *n*-dodecane, *n*-hexadecane, and bicyclohexyl were received from Fluka with a purity greater than 98% and used without further purification.

Surface Tension. Surface tension measurements were made under atmospheric pressure by the pendant drop technique as

(13) Binks, B. P.; Fletcher, P. D. I.; Sager, W. F. C.; Thompson, R. L. *Langmuir* **1995**, *11*, 977.
(14) Binks, B. P.; Fletcher, P. D. I.; Thompson, R. L. *Ber. Bunsen-Ges. Phys. Chem.* **1996**, *100*, 232.
(15) Hayami, Y.; Findenegg, G. H. *Langmuir* **1997**, *13*, 4865.
(16) Motomura, K.; Iwanaga, S.; Hayami, Y.; Uryu, S.; Matuura, R. *J. Colloid Interface Sci.* **1981**, *80*, 32. Aratono, M.; Uryu, S.; Hayami, Y.; Motomura, K.; Matuura, R. *J. Colloid Interface Sci.* **1984**, *98*, 33.
(17) Hayami, Y.; Uemura, A.; Ikeda, N.; Aratono, M.; Motomura, K. *J. Colloid Interface Sci.* **1995**, *172*, 142. Takiue, T.; Yanata, A.; Ikeda, N.; Hayami, Y.; Motomura, K.; Aratono, M. *J. Phys. Chem.* **1996**, *100*, 20122.
(18) Bothorel, P.; Such, C.; Clément, C. *J. Chim. Phys.* **1972**, *69*, 1453.
(19) Als-Nielsen, J.; Jacquemain, D.; Kjaer, K.; Leveiller, F.; Lahav, M.; Leiserowitz, L. *Phys. Rep.* **1994**, *246*, 251.
(20) Kjaer, C. *Physica B* **1994**, *198*, 100.
(21) Lang, P. In *Modern Characterization Methods of Surfactant Systems*; Binks, B. P., Ed.; Surfactant Science Series Vol. 83; Marcel Dekker: New York, 1999.
(22) Zhou, X.-L.; Chen, S.-H. *Phys. Rev. E* **1993**, *47*, 3174.
(23) Parratt, L. G. *Phys. Rev.* **1954**, *95*, 359.
(24) Kirkpatrick, S.; Gelatt, C. O.; Vecchi, M. P. *Science* **1983**, *220*, 671.
(25) Marczuk, P.; Lang, P.; Möller, M. *Colloids Surf., A* **2000**, *163*, 103.
(26) Gang, O.; Ellmann, J.; Möller, M.; Kraack, H.; Sirota, E. B.; Ocko, B. M.; Deutsch, M. *Europhys. Lett.* **2000**, *49*, 761.
(27) Höpken, J.; Pugh, C.; Richtering, W.; Möller, M. *Makromol. Chem.* **1990**, *189*, 911.

reported previously.[15] Drops of ca. 3 mm equatorial diameter were suspended from a glass rod in a closed glass cell with optically flat windows. SFA solutions were prepared by weight. Some excess amount of the solution was kept at the bottom of the cell, to saturate the vapor space with the solvent and thus to minimize its evaporation from the drop during the measurements. Drop shape measurements on drops of given SFA concentrations were made at a series of temperatures by lowering temperature in discrete steps with an equilibration time of at least 30 min at each experimental temperature. The temperature of the cell was controlled to within ±0.01 K. The drop contour was imaged by means of a CCD camera, and the surface tension was calculated from the drop shape by the selected plane method.[28] At least 300 images were analyzed and averaged for each data point. The statistical error resulting from these repeated measurements was ±0.05 mN/m, while the systematic error due to calibration and other artifacts is estimated as ±0.5 mN/m from a comparison of calibration measurements with several pure liquids with literature data.

X-ray Reflectometry. Measurements were made using a home-built reflectometer, specially designed for reflectivity measurements from the air/liquid interface. The instrument is equipped with a standard Cu tube as the X-ray source and was operated at 40 kV and 35 mA. A collimating Göbel mirror[29] (Bruker AXS, Karlsruhe, Germany) was used as the monochromator to select the Kα wavelength $\lambda = 1.54$ Å. A metal wire position-sensitive detector OED-50M (MBraun, München, Germany) was used to detect the scattered photons. The resolution of the detector was calibrated with a silver behenate powder sample.[30] The collimating system consists of two horizontal slits between the monochromator and the sample. The X-ray tube, both slits, and the detector are mounted on X-95 profiles, which are connected by a swivel joint and can be inclined independently by means of two vertical stages (type 5101, Huber Diffraktionstechnik, Rimstig, Germany). For the measurements, SFA solutions were poured onto a clean sandblasted steel plate of a covered and sealed steel cell. The temperature of the socket and the cover of the cell was controlled with an accuracy of ±5 mK by a Haake F6 bath thermostat (Haake, Karlsruhe, Germany) and monitored by a standard Pt-100 resistor. During temperature scans (reflectivity measurements at a constant incident angle), the temperature was varied in 100 steps per hour with a step width of 0.01 K.

Grazing Incidence X-ray Diffraction. GIXD experiments were conducted at the beamlines D4.1 and BW1 of the HASYLAB at DESY in Hamburg, Germany. The general setup of both instruments is described elsewhere.[19,31] For our measurements, we used a wavelength of $\lambda = 1.3037$ Å and a Soller collimator, which sets the angular resolution in the surface (q_{xy}) plane to $\Delta(2\theta) = 0.15°$. The sample environment was modified by placing the socket of the sample cell with the temperature controlling and monitoring system into a closed container with large capton windows for the incident and the scattered radiation. To improve the signal-to-noise ratio, the canister was flushed with solvent-saturated helium at the respective experimental temperature.

Results

Surface Tension Data. Figure 1 shows the temperature dependence of the surface tension γ of $F_{12}H_{18}$ solutions in dodecane for concentrations up to 3 mmol/kg. In dilute solutions (up to 0.6 mmol/kg), the surface tension exhibits a weakly negative temperature dependence over the entire experimental range. In more concentrated solutions (0.9 mmol/kg and greater), one observes a sharp transition from this $d\gamma/dT < 0$ behavior at high temperatures to a region with a positive slope at low temperatures.

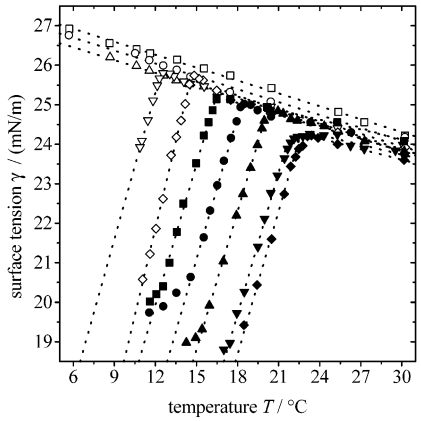

Figure 1. Surface tension γ as a function of temperature for solutions of $F_{12}H_{18}$ on dodecane. The symbols represent experimental data for different solute concentrations (○, pure solvent; △, 0.30 mmol/kg; □, 0.60 mmol/kg; ▽, 0.90 mmol/kg; ◇, 1.16 mmol/kg; ■, 1.43 mmol/kg; ●, 1.77 mmol/kg; ▲, 2.19 mmol/kg; ▼, 2.70 mmol/kg; ♦, 3.00 mmol/kg), and the dotted lines are linear least-squares fits to the branches with negative and positive slopes of the respective data set.

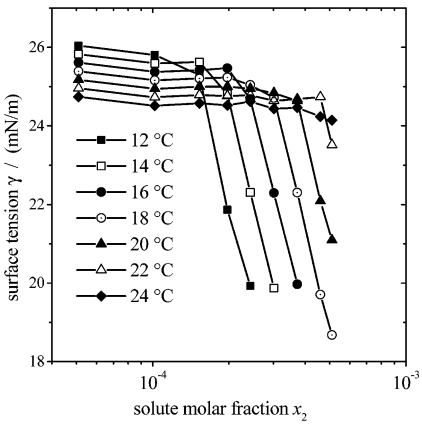

Figure 2. Surface tension γ as a function of the solute mole fraction x_2 at constant temperatures, as indicated in the legend.

The transition temperature T_f separating these two regimes increases with increasing concentration of $F_{12}H_{18}$. In the high-temperature region, γ is a linear function of temperature, and increasing the concentration at constant temperature causes a weak decrease of γ, indicating a weak adsorption of SFA at the free surface of dodecane. Below the phase transition, γ is also a linear function of T but deviations from this linear temperature dependence occur at low temperatures, presumably due to incomplete dissolution of the SFA near its solubility limit in dodecane. Only the data in the linear region, which are not affected by this artifact, were used in the data analysis. As shown by vapor pressure osmometry by Binks et al.[13] for two related systems, the SFA solutions behave ideally up to the solubility limit.

Accordingly, the relative surface excess concentration of the solute, $\Gamma_2^{(1)}$, was derived using the Gibbs equation without correction for nonideality[13,15]

$$\Gamma_2^{(1)} = -\frac{1}{RT}\left(\frac{\partial\gamma}{\partial \ln x_2}\right) \qquad (1)$$

Figure 2 shows graphs of surface tension versus mole fraction x_2 on a semilogarithmic scale. In this representation, the isotherms show two regions of constant slope $\partial\gamma/\partial \ln x_2$, and both slopes are essentially independent of temperature. These findings imply that the surface excess

(28) Andreas, J.; Hauser, E.; Tucker, W. *J. Phys. Chem.* **1938**, *42*, 1001.
(29) Bergmann, A.; Orthaber, D.; Scherf, G.; Glatter, O. *J. Appl. Crystallogr.* **2000**, *33*, 869.
(30) Huang, T. C.; Toraya, H.; Blanton, T. N.; Wu, Y. J. *J. Appl. Crystallogr.* **1993**, *26*, 180.
(31) Kjaer, C. Experimental Stations at HASYLAB; Risø National Laboratory: Roskilde, Denmark, 1994; p 88.

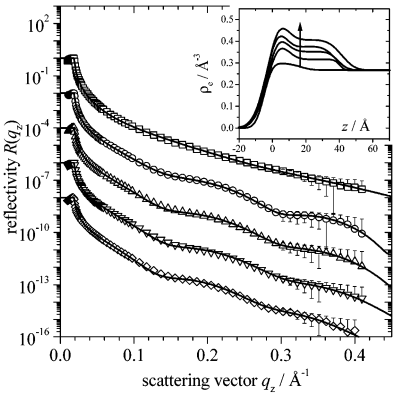

Figure 3. X-ray reflectivity $R(q_z)$ versus scattering vector q_z from the surface of a solution of 2.184 mmol/kg $F_{12}H_{16}$ in hexadecane above T_f (□) and at four different temperatures below T_f: ○, 22.3 °C; △, 20.0 °C; ▽, 19.3 °C; ◇, 17.6 °C. Symbols are experimental data, and the full lines represent best fits obtained from a two-box model of the electron density profile normal to the surface $\rho_e(z)$. The corresponding electron density distributions are shown in the inset; the arrow indicates the direction of decreasing temperature.

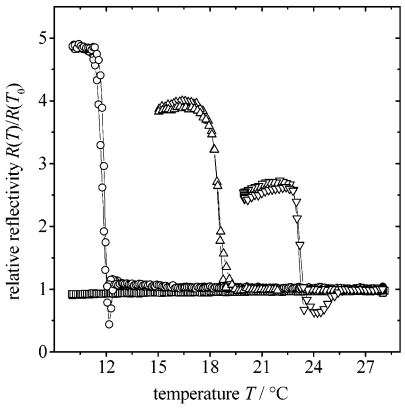

Figure 4. Relative reflectivity $R(T)/R(T_0)$ from the surface of solutions of 3.0 mmol/kg SFA in dodecane as a function of temperature at constant $q_z = 0.1$ Å^{-1}: □, $F_{12}H_{12}$; ○, $F_{12}H_{14}$; △, $F_{12}H_{16}$; ▽, $F_{12}H_{18}$.

concentration exhibits a transition from a low value ($\Gamma_2^{(1)} = 0.11 \pm 0.07$ μmol/m^2) to a high value ($\Gamma_2^{(1)} = 4.8 \pm 0.3$ μmol/m^2) as the bulk concentration is increased. On the assumption that $\Gamma_2^{(1)}$ can be identified with the absolute surface concentration, the latter value corresponds to a mean area per molecule of 34 ± 2 Å^2, which is about 20% greater than for a close-packed ordered monolayer of perfluoroalkyl chains (28 Å^2).[11]

X-ray Reflectivities. XR curves $R(q_z)$ of the surface of SFA solutions in different hydrocarbon solvents were recorded at temperatures below and above the phase transition temperature T_f of the Gibbs film. A representative example is shown in Figure 3.

Above T_f, the XR curves exhibit a monotonic decay of $R(q_z)$ at $q_z > q_c$ (critical value of total external reflection), as expected for the free surface of simple liquids. The existence of a dense Gibbs film at temperatures below T_f is indicated by a modulation of this simple decay. The transition from the high-temperature state to the low-temperature state of the film was monitored by recording the temperature dependence of the reflectivity at some fixed value of q_z at which $R(q_z)$ of the low-temperature phase deviates markedly from that of the high-temperature phase. Figure 4 shows results of such a temperature scan recorded at $q_z = 0.1$ Å^{-1} for solutions of the four

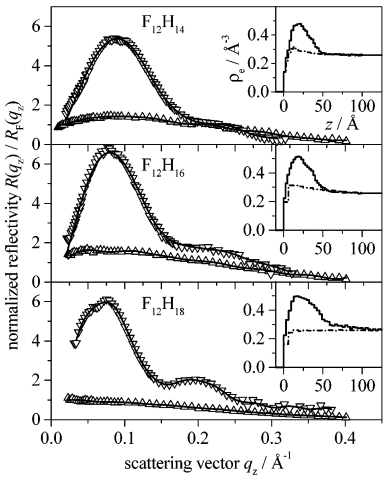

Figure 5. Reflectivity normalized to the Fresnel reflectivity of an ideal (hypothetical) pure solvent surface $R(q_z)/R_F(q_z)$ vs scattering vector q_z from the surface of three solutions of 3 mmol/kg $F_{12}H_m$ in dodecane. The data were collected 3 K above (△) and 3 K below (▽) T_f. The solid lines are best fits according to the electron density profiles displayed in the insets (full lines, low temperature; dotted lines, high temperature).

$F_{12}H_m$ materials in dodecane at a solute concentration of ca. 3 mmol/kg.[25]

For a better comparison of the four systems, the reflectivities are plotted as $R(T)/R(T_0)$, where $R(T_0)$ is the reflectivity of the respective system at a reference temperature above the phase transition. For the samples with $m = 14$, 16, and 18, the XR scans exhibit a sharp step in the experimental temperature window. The phase transition temperature T_f determined from the position of this step is reproducible, and no significant hysteresis is observed in cooling−heating cycles (Figure 4). As expected, T_f increases with the chain length of the hydrocarbon tail, suggesting that a similar phase transition will occur for $F_{12}H_{12}$ at a lower temperature.

Full XR curves of the $F_{12}H_m$ + dodecane systems ($m =$ 14, 16, and 18) recorded at temperatures ca. 3 K above and 3 K below the respective transition temperature T_f are shown in Figure 5.[25] In this figure, $R(q_z)$ is normalized to the Fresnel reflectivity $R_F(q_z)$ of an idealized surface with a step-function profile $\rho_e(z)$ changing at $z = 0$ from zero (gas phase) to the electron density of bulk dodecane. At temperatures $T > T_f$, the normalized reflectivity curves $R(q_z)/R_F(q_z)$ are nearly featureless as expected for a simple surface without adsorbed film. The respective curves for the low-temperature phase ($T < T_f$) exhibit a pronounced primary maximum and a weaker secondary maximum, which becomes more prominent as the chain length of the hydrocarbon tail increases. The reflectivity data were analyzed in terms of the electron density profile $\rho_e(z)$ on the basis of the first Born approximation. For an air/liquid interface,

$$\frac{R(q_z)}{R_F(q_z)} = \frac{1}{\rho_\infty^2}\left|\int_{-\infty}^{\infty} \frac{d\rho_e(z)}{dz} \exp\{iq_z z\}\, dz\right|^2 \qquad (2)$$

where $d\rho_e(z)/dz$ is the electron density gradient averaged over the $x-y$ plane, and ρ_∞ is the electron density in the bulk liquid phase. The density profiles derived from the model-independent analysis of the reflectivity are shown in the inset of Figure 5. The high-temperature reflectivity data ($T > T_f$) of the $F_{12}H_{18}$ system yield an almost steplike density profile rising from effectively zero (at $z \leq 0$) to the electron density of the liquid bulk phase ($\rho_\infty = 0.26$ Å^{-3}

Table 1. Relative Packing Density Θ of $F_{12}H_m$ on Dodecane and BCH[a]

m	*t*/Å	*C**/Å²	*C*/Å²	Θ = *C*/*C**
14	13.58	7.53	6.2	0.82
16	15.37	7.62	7.1	0.93
18	17.16	7.71	7.7	1.0
16 (BCH)	15.37	6.34	7.6	1.2
18 (BCH)	17.16	6.37	8.2	1.29

[a] *t* is the overall thickness of a hypothetical layer of solidlike alkane as explained in the main text. *C* and *C** are given by eqs 3 and 4. To calculate *C**, we used the electron density of the pure H_{12} solvents, i.e., $\rho_{H,l} = 0.26$ Å^{-3} for dodecane and $\rho_{H,l} = 0.30$ Å^{-3} for BCH. The uncertainties in *C* and Θ are less than ±1 in the last digit.

at $z \geq 0$). For $F_{12}H_{16}$ and $F_{12}H_{14}$ at $T > T_f$, the density profiles exhibit a weak maximum next to the surface, indicating some adsorption of these semi-fluorinated alkanes. For temperatures $T < T_f$, density profiles with a pronounced maximum, amounting to an electron density $\rho_{max} \approx 0.5$ Å^{-3}, are obtained. This value of ρ_{max} agrees with the value (≈0.52 Å^{-3}) calculated from the effective molecular area as deduced from surface tension data. However, the region of excess electron density ($\rho_e(z) > \rho_\infty$) extends to a depth of ca. 50 Å for $F_{12}H_{14}$ and $F_{12}H_{16}$. For $F_{12}H_{18}$, there is a further region of slowly decaying excess density that extends to nearly 100 Å in depth. The integrated surface excess electron density has been evaluated as

$$C = \int_0^\infty \rho_e(z) - \rho_e^0(z)\, dz \qquad (3)$$

where $\rho_e(z)$ and $\rho_e^0(z)$ are the electron density profiles as derived from the reflectivity data of the solution and pure dodecane solvent, respectively. In this relation, we neglect the small difference in the electron density of the dilute solutions and the pure solvent. In Table 1, the values of *C* derived from the experimental data on the basis of eq 3 are compared with the reference value (denoted *C**) for a monolayer of the respective $F_{12}H_m$ in which both the fluorinated and the hydrogenated blocks are close packed. Since the cross-sectional area of a hydrocarbon chain (A_H) is less than the cross-sectional area of the fluorocarbon chain (A_F), close packing of both the fluorocarbon and hydrocarbon chains of the SFA molecules implies a tilt of the hydrocarbon chains with respect to the longitudinal direction of the fluorinated chains, with a tilt angle $\phi = \arccos(A_H/A_F) \approx 45°$.

$$C^* = \rho_F l_F + \rho_{H,c} t - \rho_{H,l}(l_F + t) \qquad (4)$$

where ρ_F, $\rho_{H,c}$, and $\rho_{H,l}$ are the electron densities of close-packed fluorocarbon and alkane layers ($\rho_F = 0.67$ Å^{-3},[32] $\rho_{H,c} = 0.32$ Å^{-3} [12]) and of the liquid hydrocarbon solvent ($\rho_{H,l} = 0.26$ Å^{-3} for dodecane, $\rho_{H,l} = 0.30$ Å^{-3} for bicyclohxyl, and $\rho_{H,l} = 0.27$ Å^{-3} for hexadecane); $l_F = 16.7$ Å is the length of the extended F_{12} chain;[33] and $t = l_H \cos\phi$ the thickness of the tilted layer of hydrocarbon tails of length $l_H = (1.265m + 1.5)$ Å. Values of *C** and the quantity Θ = *C*/*C**, the relative packing density expressed in terms of a close-packed monolayer of $F_{12}H_m$, are given in Table 1. For the Gibbs films of the three $F_{12}H_m$ compounds on dodecane, at a temperature 3 K below the respective phase transition, Θ values increasing from 0.82 ($F_{12}H_{14}$) to 0.99 ($F_{12}H_{18}$) are found.

(32) Bunn, W. C.; Howell, E. R. *Nature* **1954**, *174*, 549.
(33) Birshtein, T. M.; Ptitsyn, O. B. *Conformations of Macromolecules*; John Wiley & Sons: New York, 1966.

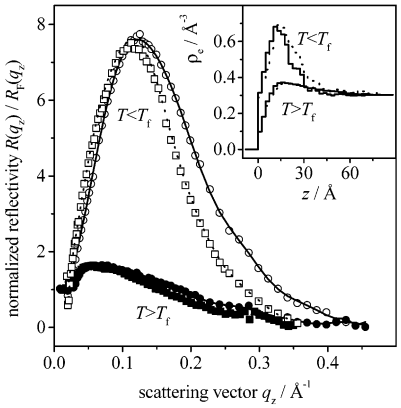

Figure 6. Reflectivity normalized to the Fresnel reflectivity of the pure solvent surface $R(q_z)/R_F(q_z)$ vs scattering vector q_z from the surface of two solutions of 1 mmol/kg $F_{12}H_m$ in bicyclohexyl. Symbols are experimental points: $F_{12}H_{16}$ (○) and $F_{12}H_{18}$ (□) 3 K below T_f; $F_{12}H_{16}$ (●) and $F_{12}H_{18}$ (■) 3 K above T_f. The lines are best fits according to the electron density profiles displayed in the inset ($F_{12}H_{16}$, full lines; $F_{12}H_{18}$, dotted lines).

XR measurements on $F_{12}H_m$ solutions in the bulky hydrocarbon BCH were made to study the influence of the hydrocarbon solvent on the properties of the Gibbs films. Since the solubility of the semi-fluorinated alkanes in BCH is less than in dodecane, solutions of 1 mmol/kg were used in these measurements. Figure 6 shows $R(q_z)/R_F(q_z)$ curves for $F_{12}H_{16}$ and $F_{12}H_{18}$ on BCH recorded at temperatures 3 K below and 3 K above the respective phase transition temperature T_f. The electron density profiles $\rho_e(z)$ were again derived from the normalized reflectivities $R(q_z)/R_F(q_z)$ by the model-independent analysis and are shown as an inset in Figure 6. At $T > T_f$, the profiles of the two systems coincide within experimental accuracy and exhibit a very weak maximum near $z = 0$, again indicating some adsorption of the $F_{12}H_m$ compounds at the surface of the liquid phase. The profiles do not exhibit a sharp step at $z = 0$ as in the dodecane systems but increase more gradually over a range of ca. 12 Å, indicating a higher surface roughness than in the case of dodecane. From the electron density profiles for the low-temperature phase ($T < T_f$) of $F_{12}H_{16}$ and $F_{12}H_{18}$, it follows that the Gibbs films on BCH are more compact than on dodecane.

Specifically, the peak value of the electron density is significantly higher ($\rho_{max} \approx 0.65$ Å^{-3}) than in the respective dodecane systems, and the thickness of the region with excess electron density is significantly smaller. This is due to the fact that the electron density difference between the hydrocarbon part of the condensed film ($\rho_{H,c} = 0.32$ Å^{-3}) and the solvent ($\rho_{H,l} = 0.30$ Å^{-3}) is much smaller than in the dodecane systems. On the other hand, the peak value of the profiles is very close to that of a hypothetical perfectly ordered F_{12} layer, indicating a very high packing density in the film. This is also brought out by the values of Θ = *C*/*C** in Table 1, which are larger than unity. Considering the simplicity of the applied model, this is clear evidence for a complete surface coverage by the solute.

Gibbs films of $F_{12}H_{16}$ on hexadecane were studied to assess the effect of the correlation of molecular orientations in the liquid state[18] on the properties of the Gibbs films. Figure 7 shows a temperature scan of the reflectivity $R(T)/R(T_0)$ recorded at $q_z = 0.2$ Å^{-1} for a solution of 2.2 mmol/kg $F_{12}H_{16}$ in hexadecane. Clearly, this system exhibits not a sharp phase transition but a gradual increase of the reflectivity over a range of several Kelvin, starting at $T_f \approx 23.5$ °C, where T_f now represents the onset temperature of the surface phase transition. On further cooling, the

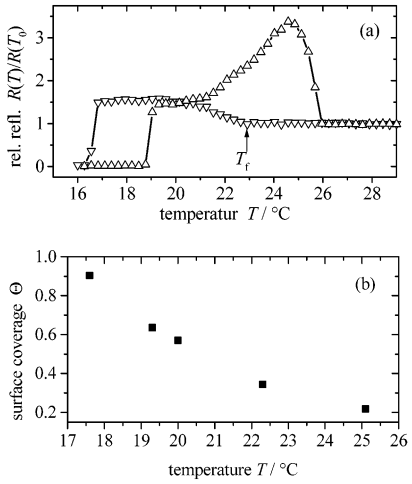

Figure 7. (a) Relative reflectivity $R(T)/R(T_0)$ at $q_z = 0.2$ Å^{-1} from the surface of a solution of 2.184 mmol/kg $F_{12}H_{16}$ in hexadecane in dependence of temperature (△, heating; ▽, cooling). The applied cooling/heating rate was 1 K/h. (b) Relative packing density Θ at selected temperatures. Θ was calculated on the basis of eqs 3 and 4 from the electron density profiles displayed in Figure 8b.

value of $R(T)/R(T_0)$ recorded at $q_z = 0.2$ Å^{-1} remains nearly constant and then falls off sharply to nearly zero at ca. 17 °C, when the bulk sample freezes. The heating curve of $R(T)/R(T_0)$ scans, when measured at a similar scanning rate as the cooling curve (ca. 1 K/min), is displaced upward by typically 2−3 K and exhibits a pronounced maximum near 25 °C, that is, ca. 2 K above T_f. This observation indicates that in this system the equilibration is quite slow in the temperature range of the surface phase transition.

Full $R(q_z)$ curves of a 2.2 mmol/kg sample of $F_{12}H_{16}$ in hexadecane are given in Figure 3. The corresponding normalized reflectivities $R(q_z)/R_F(q_z)$ are shown in Figure 8. The curve for 25.1 °C corresponds to the gaslike state above T_f, those for 22.3, 20.0, and 19.3 °C to the region assigned as the liquid expanded state in ref 15, and that for 17.6 °C to the liquid condensed state of the Gibbs film just before bulk freezing. All curves for temperatures below T_f exhibit two pronounced maxima in $R(q_z)/R_F(q_z)$. The position of these maxima is shifted toward smaller q_z and their amplitude increases as the temperature decreases below T_f, which indicates qualitatively that the thickness of the layer and the mean electron density increase in that direction. Figure 8b shows the electron density profiles derived from the reflectivity curves by the model-independent analysis. In most respects, the $\rho_e(z)$ profiles calculated by this algorithm agree well with those shown in the inset of Figure 3, which were obtained by fitting a two-box model to the reflectivity data. In all cases, the value of ρ_∞ (electron density of the bulk liquid) derived from the fitting procedure (0.27 Å^{-3}) agrees with the value calculated from the mass density of pure liquid hexadecane. The profile for 25.1 °C ($T > T_f$) comprises a surface layer of slightly enhanced electron density (0.30 Å^{-3}) which decays smoothly into the liquid phase, again indicating weak adsorption of the semi-fluorinated alkane at the surface in the temperature regime of the gaslike film above the surface phase transition. The density profiles $\rho_e(z)$ for temperatures below T_f exhibit a gradual increase of both the maximum electron density and thickness of the film with decreasing temperature. Even at the lowest accessible temperature (just before bulk freezing of the sample), the maximum electron density in the film is only ca. 0.43 Å^{-3}, that is, significantly less than for $F_{12}H_{16}$ on BCH ($\rho_{max} \approx$ 0.65 Å^{-3}) and dodecane ($\rho_{max} \approx$ 0.50 Å^{-3}). Integrated surface excess electron densities C of the $F_{12}H_{16}$ + hexadecane system were derived from the density profiles on the basis of eqs 3 and 4. Values of C and the relative packing density $\Theta = C/C^*$ for the experimental temperatures are given in Table 2 (using $C^* = 7.45$ Å^{-2} as the surface excess electron density of a perfectly ordered monolayer of $F_{12}H_{16}$ on hexadecane).

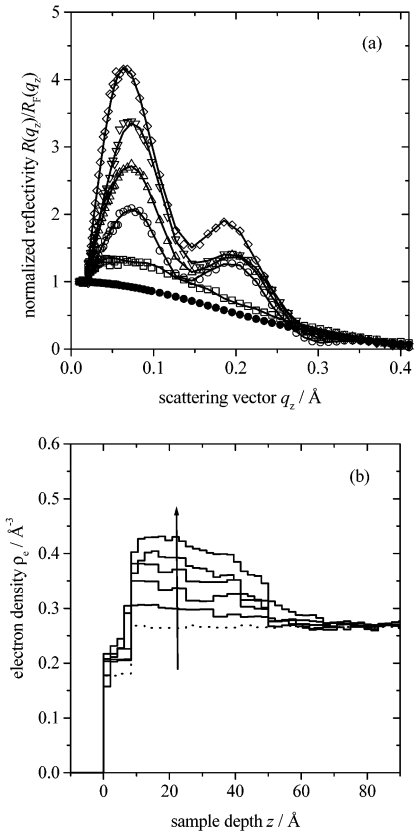

Figure 8. (a) Normalized X-ray reflectivity $R(q_z)/R_F(q_z)$ versus scattering vector q_z from the surface of pure hexadecane (●) and a solution of 2.184 mmol/kg $F_{12}H_{16}$ in hexadecane above T_f (□) and at four different temperatures below T_f: ○, 22.3 °C; △, 20.0 °C; ▽, 19.3 °C; ◇, 17.6 °C. Symbols are experimental data, and the full lines represent best fits obtained from the model-independent data analysis. (b) Corresponding electron density distributions; the arrow indicates the direction of decreasing temperature, and the dotted line corresponds to the reflectivity from the pure solvent.

Table 2. Relative Packing Density Θ of $F_{12}H_{16}$ in a Hexadecane Solution for Different Temperatures T as Calculated from Equations 3 and 4[a]

T/°C	C/Å^2	$\Theta = C/C^*$
25.1	0.9	0.12
22.3	2.6	0.35
20.0	4.0	0.54
19.3	4.9	0.66
17.6	6.7	0.90

[a] The solvent electron density is $\rho_{H,l} = 0.27$ Å^{-1} resulting in a perfect monolayer value of $C^* = 7.45$ Å^{-2}. The uncertainties in C and Θ are less than ±1 in the last digit.

From the temperature dependence of Θ in Figure 7, it is seen that the relative packing density of the film increases in a nearly linear way below T_f over the entire experimental range, reaching a value of ca. 0.9 at the lowest accessible temperature. The fact that the scan of $R(T)/R(T_0)$ unlike Θ does not continue to increase but reaches a plateau value below 20 °C is an artifact, since $R(T)/R(T_0)$ is no longer a measure of the surface excess

Table 3. Lattice Parameters of the Two-Dimensional $F_{12}H_m$ Monolayers on Top of Dodecane and BCH as Determined by GIXD[a]

m	T/°C	q_{xy}/Å^{-1}	d_{10}/Å	A/Å^2	fwhm/Å^{-1}	ξ/Å	N
14	11	1.26 ± 0.01	4.97 ± 0.05	28.5 ± 0.3	0.074 ± 0.003	17 ± 0.8	3.4 ± 0.2
16	15	1.26 ± 0.01	4.98 ± 0.05	28.6 ± 0.3	0.066 ± 0.003	19 ± 0.8	3.7 ± 0.2
18	21	1.26 ± 0.01	4.96 ± 0.05	28.4 ± 0.3	0.059 ± 0.003	21 ± 0.8	4.2 ± 0.2
18 (BCH)	20	1.26 ± 0.01	4.96 ± 0.05	28.4 ± 0.3	0.060 ± 0.003	20 ± 0.8	4.1 ± 0.2

[a] T is the experimental temperature, q_{xy} is the position of the Bragg peak as depicted in Figure 9, d_{10} is the corresponding lattice spacing, A is the resulting area per molecule, fwhm is the full width at half-maximum of the peak, ξ is the corresponding correlation length, and N is the respective number of coherently scattering lattice lines. The error limits result from the uncertainties of the fits of a Gaussian to the in-plane peaks.

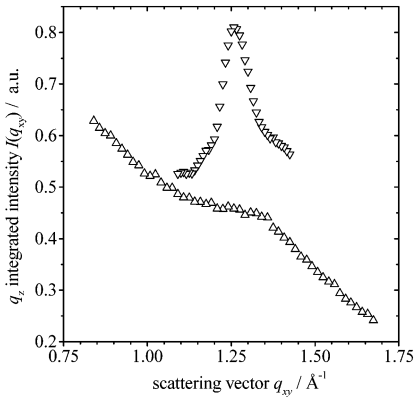

Figure 9. One-dimensional grazing incidence diffraction patterns from the surface of the $F_{12}H_{16}$ + dodecane system at 25 °C (△) and at 15 °C (▽). The symbols are scattered intensities integrated along the q_z direction over $0 \le q_z \le 0.1$ Å^{-1}.

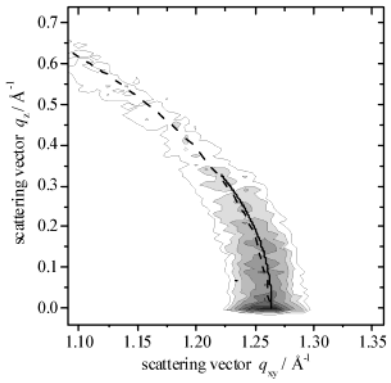

Figure 10. Two-dimensional contour plot of the GIXD intensity from the surface of the $F_{12}H_{16}$ + dodecane system below T_f. The data were corrected for the solvent background scattering. The dashed line is a circular arc according to eq 5 with $d_{10} = 4.98$ Å. The full line is calculated using the exact expression of ref 37 using $\Phi = 16°$ and a random distribution of the tilt azimuth.

concentration of the adsorbed SFA when the thickness and density of the film (and thus the amplitude and the wavelength of the undulations in the reflectivity curve, see Figure 8) vary with temperature, as in this case.

Grazing Incidence Diffraction. GIXD was used to elucidate the lateral structure of the monolayer films. The general appearance of the recorded diffraction patterns was similar for all systems studied. The scattered intensity $I(q_{xy})$ was derived by integrating over the q_z dependence of the scattered intensity in a range $0 \le q_z \le 0.1$ Å^{-1}. As a representative example, Figure 9 shows $I(q_{xy})$ for a solution of 3 mmol/kg $F_{12}H_{16}$ in dodecane. Above the surface phase transition temperature ($T_f \approx 18$ °C), $I(q_{xy})$ falls off in a monotonic way, except for a broad halo around $q_{xy} = 1.37$ Å^{-1}, which is characteristic of liquid *n*-alkanes.[34]

Below the surface phase transition, a single pronounced diffraction peak appears in $I(q_{xy})$ which was fitted by a Gaussian. The d_{10} spacing of the corresponding 2D lattice is obtained from the position of the Bragg peak as $d_{10} = 2\pi/q_{xy}$, and the area per molecule A is given by $A = 2d_{10}^2/\sqrt{3}$. Results for d_{10} and A for the present systems are summarized in Table 3. It is seen that $d_{10} = 4.97 \pm 0.01$ Å for all $F_{12}H_m$ materials on both H_{12} solvents. Slightly higher values, $d_{10} = 5.02 \pm 0.05$ Å, were found for two further semi-fluorinated alkanes, $F_{14}H_{14}$ and $F_{14}H_{16}$, on dodecane at 20 and 24 °C, respectively.[35]

For the present systems, the GIXD Bragg peaks are rather broad. The full width at half-maximum (fwhm) of the peaks is ca. 0.06 Å^{-1}, that is, a factor of 6 greater than the instrumental resolution ($\delta q_{xy} \approx 0.01$ Å^{-1}). Accordingly, the fwhm is a measure of the positional correlation length ξ of the molecules in the film, which can be estimated by the relation $\xi = 0.9\lambda/(\text{fwhm} \cos\theta_c)$, where θ_c is the position of the peak center.[36] Values of the correlation length derived in this way (Table 3) are typically of the order 20 Å, corresponding to just a few coherently scattering lattice lines in the film. For the systems studied in this work, it is found that ξ increases somewhat with the length of the hydrocarbon tail of the $F_{12}H_m$ molecules. Very similar values of ξ are found for $F_{12}H_{18}$ in the two H_{12} solvents.

Figure 10 shows the GIXD intensity of the $F_{12}H_{16}$ + dodecane system mapped in a two-dimensional (q_{xy} vs q_z) contour plot. In such a diagram, the scattered intensity is found along the rim of a circle centered at $q_{xy} = q_z = 0$ of radius $\sqrt{(q_{xy}^2 + q_z^2)} = 1.262$ Å^{-1}. Weidemann et al.[37] have shown that this kind of scattering pattern can be explained by a 2D arrangement of cylinders which are tilted with respect to the surface normal, if the polar tilt angle Φ and/or the tilt azimuth Ψ are distributed randomly. For such a geometry, the magnitude of the scattering vectors parallel and perpendicular to the surface plane, q_{xy} and q_z, are related to the lattice constant d_{10} in the surface plane approximately by

$$q_{xy}^2 + q_z^2 = \frac{4\pi^2}{d_{10}^2} \qquad (5)$$

The dashed line in Figure 10 shows this relation using $d_{10} = 4.98$ Å as derived from the peak position in Figure 9. As explained earlier, the difference in the cross-sectional areas of the F and H blocks of the $F_{12}H_m$ molecules causes a tilt of the blocks with respect to each other. If the F blocks of all molecules were oriented surface normal and the H blocks were tilted with a random tilt azimuth, then one should find an intense Bragg rod resulting from the

(34) Wu, X. Z.; Sirota, E. B.; Sinha, S. K.; Ocko, B. M.; Deutsch, M. *Phys. Rev. Lett.* **1993**, *70*, 958.
(35) Marczuk, P. Ph.D. Thesis, Technische Universität Berlin, Berlin, Germany, 2000.
(36) Warren, B. E. *X-ray Diffraction*; Dover: New York, 1990.
(37) Weidemann, G.; Brezesinski, G.; Vollhardt, D.; Möhwald, H. *Langmuir* **1998**, *14*, 6485. Weidemann, G.; Brezesinski, G.; Vollhardt, D.; De Wolf, C.; Möhwald, H. *Langmuir* **1999**, *15*, 2901.

F block, with a half-width in the z direction corresponding to the length of the F block (i.e., $0.2-0.3$ Å^{-1}), superimposed on a weak ring resulting from the tilted H blocks. The GIXD contour in Figure 10 does not support such a structure model of vertically oriented F blocks, as the diffracted intensity appears to be distributed along a curve, even for small values of q_z.

From the fact that the cross-sectional area of the F_{12} blocks in the film exceeds the respective value for poly(tetrafluoroethylene) (PTFE) (27.4 Å^2 [32]) by ca. 4%, one estimates a tilt angle of the F blocks Φ_F against the surface normal of 16°. The exact relation between q_z and q_{xy} (eqs 4 and 12 in ref 37a) yields the full line in Figure 10 for this value of Φ_F, if a random distribution of the tilt azimuth is assumed. This model could explain in part the very high degree of disorder in the Gibbs film.

Discussion

$F_{12}H_m$ Films on H_{12} Solvents. The results of this study confirm earlier reports that Gibbs films of semi-fluorinated alkanes at the surface of liquid hydrocarbons may exhibit a sharp phase transition from a gaslike state to a dense monolayer phase. For the present series of $F_{12}H_m$ molecules (m = 14, 16, 18), a sharp surface phase transition is observed for solutions in dodecane and bicyclohexyl. This transition is seen in the temperature dependence of the surface tension as well as the X-ray reflectivity. The integral surface excess electron density C derived from the reflectivity data indicates that this transition occurs from a dilute gaslike film above the transition temperature T_f to a nearly close-packed monolayer below T_f. The packing of the molecules in the film is characterized by the relative packing density $\Theta = C/C^*$, which relates the packing density of the real film to that of a hypothetical perfectly ordered close-packed monolayer in which the hydrocarbon tails of the SFA molecules are tilted by ca. 45° to allow a close packing of both the fluorocarbon and hydrocarbon chains. In the series of $F_{12}H_m$ compounds on dodecane, Θ increases from ca. 0.8 ($F_{12}H_{14}$) to 1.0 ($F_{12}H_{18}$) (Table 1). This increase of Θ with the length of the hydrocarbon tails of $F_{12}H_m$ molecules can be attributed to an increasing attractive lateral interaction between hydrocarbon tails in the film, which stabilizes a dense Gibbs film. The same trend of Θ with increasing hydrocarbon chain length is seen for $F_{12}H_{16}$ and $F_{12}H_{18}$ on BCH.

For given members of the $F_{12}H_m$ family, the properties of the low-temperature phase at the surface of dodecane and BCH are not much different. One notes that for both $F_{12}H_m$ compounds for which such a comparison has been made, higher values of Θ are found for the adsorption from the globular hydrocarbon (BCH) in comparison with the linear-chain alkane (dodecane). We attribute this difference to the different strength of interaction of $F_{12}H_m$ molecules with the two solvents: Specifically, a more attractive interaction of dodecane, in comparison with BCH, with the alkane blocks of the $F_{12}H_{16}$ and $F_{12}H_{18}$ molecules may be due to a correlation of molecular orientations between hydrocarbon chains of the solvent and the solute in dodecane. This effect is expected to be even stronger in the case of $F_{12}H_{16}$ in hexadecane where the free energy penalty due to the chain length mismatch vanishes,[38] because the chain length of the solvent matches the length of the hydrocarbon tails of the $F_{12}H_{16}$ molecules. We return to this point later.

The GIXD results indicate a 2D hexagonal packing of the F blocks in the plane perpendicular to the block axis, which may however be tilted by a small tilt angle $\phi \leq 16°$ with respect to the surface normal. The lattice spacing d_{10} is 4.97 ± 0.01 Å, independent of the chain length of the $F_{12}H_m$ compounds. This value is about 2% larger than the lattice spacing in PTFE (d_{10} = 4.87 Å[32]) and the high-temperature bulk phase of pure $F_{12}H_m$ compounds with $m < 14$.[11] The area per molecule in the close-packed phase of the Gibbs film as obtained from the GIXD measurements, $A = 2d_{10}^2/\sqrt{3} = 28.6$ Å^2, is similar to the 27.6 Å^2 observed for the surface-frozen layer of the pure SFA.[26] However, it is significantly lower than the mean area of 34 ± 2 Å^2 derived from the surface tension isotherms of $F_{12}H_{18}$ on dodecane. We attribute this difference to the short-range nature of the positional order in the Gibbs monolayer. Table 3 shows that the in-plane positional correlation length ξ is of the order of 20 Å, that is, smaller by several orders of magnitude than in the surface-frozen monolayer of long-chain n-alkanes.[12] Table 3 also indicates that ξ increases somewhat with the chain length of the $F_{12}H_m$ molecule and is not significantly affected by the nature of the hydrocarbon solvent. Although not very pronounced, both of these effects are in line with the trends observed for the relative packing density Θ (Table 1).

The electron density profiles $\rho_e(z)$ derived from the XR curves of the present systems generally exhibit a maximum near the outer surface of the film (see, for instance, Figure 3) indicating that the $F_{12}H_m$ molecules are oriented with the F_{12} block pointing to the vapor phase. The excess electron density is smeared out over a width of ca. 40 Å for the films on BCH (Figure 6) and at least 50 Å for the films on dodecane (Figure 5). Since the excess electron density arises almost entirely from the fluorinated block, which has a length of 16.7 Å, the centers of the F_{12} blocks in the film cannot be aligned in a plane but must be distributed over a region of 20−30 Å in the z direction, like in a *smectic C* film. Such an up−down staggering of the molecules over a lateral length scale of either a single or several molecular diameters has been observed in bulk perfluoralkanes[39] in the low-temperature solid phases of the pure $F_{12}H_m$ with m = 8, 10, and 12[11] and for the surface-frozen layer of pure $F_{12}H_8$ and $F_{12}H_{14}$.[26] One may speculate further that staggering of tilted segments leads to a local buckling of the SFA layer, as suggested for the surface-frozen layer of $F_{12}H_{19}$.[26]

$F_{12}H_{16}$ on H_{16}. Gibbs films of $F_{12}H_{16}$ on hexadecane exhibit a more complex behavior than observed with any of the $F_{12}H_m$ compounds on dodecane or BCH. From the temperature dependence of Θ (Figure 7), it is seen that the transition from the gaslike state at high temperature to a condensed monolayer does not occur *in one step*, as in the adsorption from dodecane (Figure 4). Instead, Θ increases gradually as the temperature decreases below 23.5 °C, and a surface concentration corresponding to a close-packed monolayer ($\Theta \approx 1$) has not been reached when freezing of the bulk sample occurs at 17.6 °C. The absence of a phase transition of the Gibbs film in this system cannot be due solely to the solute, as the films of $F_{12}H_{16}$ on dodecane and BCH do exhibit a sharp phase transition. Obviously, the properties of the solvent H_{16} and the interactions between $F_{12}H_{16}$ and H_{16} must play a role.

We conjecture that the absence of a first-order phase transition in this system is a consequence of the strong attractive lateral interaction between H_{16} chains when they are arranged side-by-side in their all-trans conformation. This lateral interaction between higher n-alkane molecules is the main cause for the surface-freezing at

(38) Wu, X. Z.; Ocko, B. M.; Tang, H.; Sirota, S. B.; Sinha, S. K.; Deutsch, M. *Phys. Rev. Lett.* **1995**, *75*, 1332.

(39) Strobl, G.; Elben, H.; Jaeger, R.; Kimmig, M.; Steiner, R.; Schwickert, H.; Ritter, C. *J. Chem. Phys.* **1991**, *95*, 2807.

the free liquid surface[12,40,41] and a related prefreezing phenomenon at the interface against atomically flat surfaces such as graphite.[42,43] Surface-freezing requires a minimum chain length of 15 (theoretical prediction) to 16 (experimental data) carbon atoms for pure alkanes.[12] A partial alignment of alkane chains, similar to the correlation of molecular orientations of long-chain *n*-alkanes in the pure liquid state,[18] is expected to occur between the H_{16} tail of $F_{12}H_{16}$ molecules and the H_{16} solvent. This effect can be seen as a solvation of the oleophilic block of SFA in alkane solvents. It is expected to be more pronounced in hexadecane than in dodecane, as the length of the H_{16} molecule (ca. 22 Å) matches that of the alkane blocks of $F_{12}H_{16}$. For geometrical reasons, such a solvation of the $F_{12}H_{16}$ molecules does not permit a close packing of their F_{12} blocks in the Gibbs film. As the energy gain of the close packing of the fluoroalkane blocks of SFA is thought to be the main driving force for their surface phase transition at T_f, the solvation of the alkane block by $F_{12}H_{16}$ can prevent a sharp (first-order) phase transition. In this case, the energy gain connected with the microphase separation of alkane and fluoroalkane blocks will cause a gradual increase of the surface concentration of SFA with decreasing temperature, as observed for $F_{12}H_{16}$ in H_{16} solutions.

As in solutions of the H_{12} solvents, the excess electron density of the Gibbs films of $F_{12}H_{16}$ on H_{16} is smeared out over a region broader than the length of the F_{12} block, indicating a staggering of the molecules. A detailed interpretation of the $\rho_e(z)$ profiles of this system (Figure 8b) in terms of the packing of the molecules is not possible. In particular, it is not known if, or to what extent, desolvation of the alkane blocks and close packing of the fluorocarbon blocks (possibly connected with a tilting and close packing of the alkane blocks) occur as the temperature is lowered. In particular, the origin of the long-range tail of $\rho_e(z)$ seen at the lowest experimental temperature (17.6 °C) is not known.

In the earlier study of the $F_{12}H_{16}/H_{16}$ system,[15] the evolution of surface states was monitored by surface tension measurements in a temperature range from 16 to 40 °C and for $F_{12}H_{16}$ concentrations up to 5 mmol/kg. The results were summarized in a $\gamma-T$ phase diagram (Figure 6 in ref 15) showing the putative regions of stability of the surface-frozen phase of $F_{12}H_{16}$ and of three monolayer phases of $F_{12}H_{16}$ (gaslike, liquid expanded, and condensed). According to that phase diagram, surface-freezing of H_{16} occurs at the surface of dilute solutions ($c < c_E \approx 1.3$ mmol/kg) at temperatures below the surface-freezing temperature of pure $F_{12}H_{16}$ (17.6 °C), but a transition from the gaslike phase to the condensed phase of $F_{12}H_{16}$ occurs at concentrations $c > c_E$. For even higher concentrations ($c > c_T \approx 1.4$ mmol/kg), it was concluded that the transition from the gaslike to the condensed phase of the Gibbs films involves two distinct surface phase transitions, with a liquid expanded phase existing in the temperature range from T_f (gas/liquid expanded transition) to T_c (liquid expanded/condensed transition). In light of the present work, this putative phase diagram has to be modified in the sense that at concentrations $c > c_T$ the transition from the gaslike to the condensed state of the film proceeds in a continuous way as the temperature is lowered. No XR data exist for more dilute concentrations ($c < c_T$) for which the phase diagram predicts a single first-order phase transition. In that case, the coexistence line of the gaslike and condensed phases would terminate in a 2D critical point (instead of the triple point of the putative phase diagram). Alternatively, the transition from the gaslike to the condensed state of the Gibbs film may be continuous down to the lowest experimental temperatures. Further XR measurements for dilute sulutions of $F_{12}H_{16}$ in H_{16} are needed to resolve this question.

Conclusions

We have studied Gibbs films of $F_{12}H_m$ ($m = 12, 14, 16, 18$) at the free liquid surface of their solutions in two *n*-alkanes (dodecane and hexadecane) and in bicyclohexyl. For the two H_{12} solvents, sharp first-order phase transitions from a gaslike to a condensed state of the Gibbs film were observed. For H_{16}, however, which shows surface-freezing in the pure state, a gradual transition from the gaslike to the condensed state of the film was found. This different behavior is explained tentatively in terms of three types of interactions in those systems: (a) the mutual antipathy between hydrocarbon and fluorocarbon chains, which drives the adsorption of the SFA molecules at the surface of the solutions in alkanes; (b) the attractive lateral interaction between the fluorocarbon blocks of the SFA molecules in the surface; and (c) the related effect of a strong lateral interaction between the hydrocarbon block of the SFA molecules and long-chain alkanes such as H_{16} (and, to a much lesser degree, H_{12}), which causes a solvation of the alkane block of the SFA. These effects, in combination with the geometrical incompatibility between the two blocks of SFA molecules, can explain the main features observed in this study.

The Gibbs films of $F_{12}H_m$ with $m \geq 14$ on dodecane and bicyclohexyl, which show first-order phase transitions at a concentration-dependent temperature T_f, form a condensed phase in which the F_{12} blocks are arranged in 2D hexagonal arrays, with a small tilt angle against the surface plane ($\Phi \leq 16°$). The hexagonal order persists on short length scales only, with an in-plane positional correlation length of only a few molecular diameters. Furthermore, the electron density profiles indicate that the centers of mass of the F_{12} blocks are not arranged in a plane but spread out over some distance, possibly due to a staggered arrangement of the molecules.

The anomalous behavior of the Gibbs films of $F_{12}H_{16}$ on H_{16}, for which a continuous transition from the gaslike to the condensed film is observed, is attributed to the solvation of the alkane block of the SFA by the hydrocarbon solvent. This system shows that this solvation effect can have a pronounced effect on the state of Gibbs films and may induce qualitative changes of the phase behavior of such systems.

Acknowledgment. We thank K. Kjaer for his help at the BW1 beamline of HASYLAB/DESY in Hamburg. This work was supported by the DFG through the Sfb 448 and through the Schwerpunktprogramm "Benetzung und Strukturbildung an Grenzflächen" (Fi 235/13).

LA025596D

(40) Earnshaw, J. C.; Hughes, C. J. *Phys. Rev. A* **1992**, *46*, R4494.
(41) Deutsch, M.; Wu, X. Z.; Sirota, E. B.; Sinha, S. K.; Ocko, B. M.; Magnussen, O. M. *Europhys. Lett.* **1995**, *30*, 283.
(42) Kern, H.; v. Rybinski, W.; Findenegg, G. H. *J Colloid Interface Sci.* **1977**, *59*, 301.
(43) Grosse-Rhode, M.; Findenegg, G. H. *J Colloid Interface Sci.* **1978**, *64*, 374.